Reports of Biochemistry & Molecular Biology
Vol.8, No.4, Jan 2020

Original article

www.RBMB.net

Recombinant Expression and Purification of Extracellular Domain of the Programmed Cell Death Protein Receptor

Adish Zhansaya*[1,2], Mukantayev Kanatbek[1], Tursunov Kanat[1], Ingirbay Bakhytkali[1], Kanayev Darkhan[1], Kulyyassov Arman[1], Tarlykov Pavel[1], Mukanov Kasym[1], Ramankulov Yerlan[1]

Abstract

Background: The programmed cell death protein 1 (PD-1), which is a member of the CD28 receptor family, can negatively regulate antitumor immune responses by interacting with its ligands, PD-L1 or PD-L2. The PD-1–PD-L1 signaling pathway is a checkpoint mechanism that plays essential roles in downregulating immune responses in cancerous tissues. Thus, blocking this signaling pathway leads to enhanced antitumor immunity, potentially preventing tumor progression.

Methods: We synthesized the extracellular domain of the PD-1 receptor (rPD-1) de novo by using a two-step polymerase chain reaction and the Phusion® DNA polymerase. The synthesized gene was cloned into the pET28 expression plasmid and transformed into competent *Escherichia coli*. Purification of rPD-1 was performed by metal-affinity chromatography, using a HisTrap column. Purified rPD-1 was characterized by western blotting and mass spectrometry using the SwissProt database and the Mascot program.

Results: Designed and synthesized construct of rPD-1 was 500 bp in size. Analysis of the electrophoresis data of purified rPD-1 showed the presence of a protein with a molecular mass of 21 kDa. Mass spectrometry data using the SwissProt database and the Mascot program outputted the highest-scoring sequence to correspond to rPD-1.

Conclusions: Synthesized de novo rPD-1 may have potential therapeutic applications in enhancing antitumor immune responses.

Keywords: Cancer, PD-1 ligands, PD-1 receptor, Tumor immunotherapy.

Introduction

The programmed cell death protein 1 (PD-1) receptor of T-cells is a regulator that can activate or repress immunological responses depending on the underlying context (1). The primary physiological role of the PD-1 receptor is to cause T-cell apoptosis under high activity of the immune system in the body, thus preventing autoimmune reactions. Similarly, the signaling pathways through the PD-1 receptor play essential roles in the regulation of immunity against infection. For example, in mice lacking CD4+ helper T-cell and chronically infected with lymphocytic choriomeningitis virus, blockade of the inhibitory PD-1–PD-L1 signaling restores CD8+ T-cell ability to proliferate, secrete cytokines, kill infected cells, and reduce the viral load (2, 3). PD-1, in its immune-checkpoint capacity, can affect tumor growth. Tumor cells can inhibit anti-cancer immunity and avoid attacks by cytotoxic T-cells by downregulating cytotoxic T-lymphocyte antigen 4 (CTLA-4), T-cell immunoglobulin mucin-3 (TIM3), 2B4 (CD244), B- and T-lymphocyte attenuator (BTLA), lymphocyte-activation gene 3 (LAG3), PD-1, programmed cell death ligand 1 (PD-L1), and programmed cell death ligand 2 (PD-L2) (4).

1: National Center for Biotechnology, Kurgalzhyn road, 13/5, Astana, 010000, Kazakhstan.
2: L. N. Gumilyov Eurasian National University, Satpayev st., 2, Astana, 010008, Kazakhstan.
***Corresponding author: Adish Zhansaya; Tel: +77 172 707527, Fax: +77 172 707564; E-mail: zhansaiya. adish@mail.**
Received: 14 Aug, 2019; Accepted: 29 Aug, 2019

PD-1 is a type -I membrane protein that belongs to the CD28 immunoglobulin superfamily and represents the transmembrane proteins containing an extracellular IgV-like N-terminal domain, a transmembrane domain, and a cytoplasmic tail. PD-1 contains 288 amino acids, translating into a 55-kDa protein. The cytoplasmic domain of PD-1 contains two amino acid domains defined as a tyrosine-based inhibitory motif and a tyrosine-based switch motif. The amino acid sequence of its C-terminal tyrosine-based domain (TEYATIVF) interacts with protein-tyrosine phosphatase 1 (SHP-1) and protein-tyrosine phosphatase 2 (SHP-2). Tyrosine phosphorylation and dephosphorylation of proteins underlie critical regulatory events of many signaling pathways that lead to cell proliferation, differentiation, and cell death (5-7).

PD-1 is expressed on activated cells of the immune system, such as CD4+ T-cells, CD8+ T-cells, B-cells, killer T-cells, monocytes, dendritic cells, and macrophages. Moreover, expression of PD-1 is increased selectively in T-cells subjected to prolonged exposure to antigens and is a marker of depleted T-cells and cells with impaired effector functions (8, 9). PD-1 expression is regulated by interleukins, such as IL-6 and IL-10, which enhance PD-1 expression on CD8+ T-cells and that of PD-L1 on cancer cells (6, 7). Herewith, PD-L1 expression on circulating monocytes positively correlates with PD-1 expression on circulating CD4+ or CD8+ T-cells. Cumulative literature suggests that several common factors increase expression of PD-1 and PD-L1 concomitantly. Moreover, PD-1 expression was found to be higher in resident CD4+ and CD8+ T-cells in gastric cancer than those circulating in the peripheral blood or residing in normal gastric mucosa. These findings suggest that cancer cells can influence PD-1 and PD-L1 expression in gastric cancer. PD-1 expression is regulated by the transcription factor T-bet, which was described in the context of activation of antiviral CD8+ T-cells in chronic infections. The relationship between T-bet and PD-1 may depend on the state of the immune response against viral infection (4, 10).

Of the two ligands of PD-1, PD-L1 is a transmembrane glycoprotein of 290 amino acids, which belongs to the B7–CD28 immunoglobulin superfamily (10, 11). Inhibition of PD-1–PD-L1 interaction by therapeutic antibodies, such as Pembrolizumab, Nivolumab, or Atezolizumab, can effectively treat several cancer types, including melanoma, renal cell carcinoma, small-cell lung carcinoma, urothelial carcinoma, and head-and-neck carcinomas (12-15). Thus, long-term effects of immune checkpoints in typically lethal cancers have generated widespread, intense interest in cancer immunotherapy (16, 17).

However, according to Maute *et al*., therapeutic antibodies have certain disadvantages, including large size, inefficient tissue infiltration, and interaction with T-cells in tumor tissues. An additional limitation of antibodies is their activation of cytotoxic immune responses by cytotoxic T-cells and macrophages, thus decreasing the number of helper T-cells. Accordingly, we propose that a small, soluble ectodomain of PD-1 may act as a competitive antagonist, potentially inhibiting PD-1–PD-L1 interaction. At ~14 kDa, the PD-1 ectodomain is about 10-fold smaller than a monoclonal antibody (~150 kDa) and it also lacks the Fc fragment of an antibody (18). To test this hypothesis, we expressed and purified the human PD-1's extracellular domain. Here, we report expression, purification, and characterization of this recombinant protein (designated as rPD-1).

Materials and methods

Bacterial strain, plasmids, and antibodies

E. coli DH5α, BL21 (DE3) (Novagen, USA), and plasmids pGEM-TEasy (Promega, USA) and pET28 (Novagen, USA) were used. *E. coli* were maintained in LB medium. Western blotting used a mouse monoclonal antibody against His-tag and peroxidase-conjugated secondary antibodies.

Gene synthesis

Oligonucleotides (Table 1) were synthesized in the laboratory of organic synthesis of Republican State Enterprise "National Center for Biotechnology" under the Science Committee of the Ministry of Education and Science of the Republic of Kazakhstan. The amino acid sequence of rPD-1 was extracted from PubMed with NCBI sequence reference NP_005009.2. For synthesizing the *rPD-1* gene, a two-step

PCR using the Phusion® High-Fidelity DNA Polymerase was performed (Thermo Fisher Scientific). The conditions and the number of PCR cycles were the same for the combined assembly steps and amplification steps. The manufacturer recommended that the total PCR time for this polymerase is 1 min and 10 s; i.e., we programmed 10 s at 95 °C, 30 s at 55 °C, and 30 s at 72 °C. The gene sequence was optimized for expression in *E. coli* using the pET28 plasmid and was cloned using the EcoRI and XhoI restriction sites. The final pET28 plasmid construct contained a thrombin site, the extracellular domain of the PD-1 receptor, and six His-Tags. The predicted molecular weight of the His-tagged rPD-1 was ~21 kDa.

Table 1. Oligonucleotides used in the synthesis of rPD-1

Name	Nucleotide sequence
PD1 1	GGATCCGAATTCCCATGGGACTGGATAGC
PD1 2	AGCGCCGGAGAAAAGGTCGGCGGGTTCCACGGGCGATCCGGGCTATCCAGTCCCATGGGA
PD1 3	ACCTTTTCTCCGGCGCTGCTGGTGGTGACCGAAGGCGATAACGCGACGTTTACCTGCAGC
PD1 4	GCGATACCAGTTCAGCACAAAGCTTTCGCTGGTGTTGCTAAAGCTGCAGGTAAACGTCGC
PD1 5	TGTGCTGAACTGGTATCGCATGAGCCCGAGCAACCAGACCGATAAACTGGCGGCGTTTCC
PD1 6	AACGCGGAAGCGGCAATCCTGACCCGGCTGGCTGCGATCTTCCGGAAACGCCGCCAGTTT
PD1 7	TGCCGCTTCCGCGTTACCCAGCTGCCGAACGGCCGCGATTTTCATATGAGCGTGGTTCGT
PD1 8	CGCACCGCACAGATAGGTGCCGCTATCGTTGCGGCGCGCACGAACCACGCTCATATGAAA
PD1 9	CCTATCTGTGCGGTGCGATTAGCCTGGCGCCGAAAGCGCAGATTAAAGAAAGCCTGCGTG
PD1 10	TCGGCACTTCCGCACGACGTTCCGTCACGCGCAGTTCGGCACGCAGGCTTTCTTTAATCT
PD1 11	CGTGCGGAAGTGCCGACCGCGCATCCGAGCCCGTCTCCGCGCCCGGCGGGCCAGTTCCAG
PD1 12	AGAAGCTTCTCGAGTTAATGATGATGATGATGATGCTGGAACTGGCCCGCC
PD1 start	GGATCCGAATTCCCATGGGACT
PD1 stop	AGAAGCTTCTCGAGTTAATG

Transformation of E. coli and expression of rPD-1

Competent BL21 (DE3) *E. coli* were transformed with the pET-28 plasmid vector, with or without the gene insert, by electroporation using a MicroPulser (Bio-Rad) under the following conditions: 100 ng of plasmid per 50 μL of cell suspension, at 2.5 kV, 25 μF, and 200 Ω. The electroporation duration was 5.0 ms. The transformed cells were incubated in 950 μL of super optimal broth (SOC) at 37 °C for 1 h with rotary shaking at 150 rpm. Then, 50 μL of cells were seeded onto LB agar containing kanamycin as the selection antibiotics and grown at 37 °C for 16 h. Single colonies of transformants were cultured in LB broth containing kanamycin. In the middle of the logarithmic growth phase of the bacterial mass (absorbance at λ=600 nm, OD 600 = 0.6), 0.1 mM of the inducer, isopropyl-β-D-1-galactopyranoside (IPTG), was added and culture incubated for 16 h. Cells were precipitated by centrifugation at 6,000 ×*g*, 4 °C, 7 min.

For sequencing, the *rPD-1* gene product was cloned in the pGEM-T plasmid and transformed into the DH5α *E. coli* strain. *E. coli* colonies were grown on solid agar medium and analyzed by PCR using the *Taq* polymerase and M13 primers. Four positive clones were used for DNA purification and sequencing. The BigDye Terminator reagent kit (Thermo Fisher Scientific, USA) was used for sequencing.

Cell lysis and chromatographic purification

Cells were lysed using a UP200S ultrasonic disintegrator used at 24 kHz in a pulsating mode (10 pulses, 10 s per pulse) on an ice-cold buffer (20 mM NaCl, 20 mM HEPES, and 0.1 mM phenylmethylsulfonyl fluoride, pH 7.5). Recombinant protein was purified using metal-chelate chromatography on Ni^{2+} ions using a 1-mL HisTrapTM HP column (GE Healthcare, USA). First, the insoluble material was pelleted by centrifugation and removed. The protein solution was loaded onto $Ni2^{+}$-NTA column (2 mL bed volume) and equilibrated with the same buffer. The column was washed with 10 bed volumes of the equilibration buffer (20 mM Tris-HCl, pH 8.0, containing 8 M urea, 500 mM NaCl, 20 mM imidazole). For refolding of the resin-bound protein, a linear gradient of urea (8–0 M) was run

through 30 mL at 0.5 mL/min. The refolded rPD-1 was finally eluted using a linear gradient of imidazole (20–500 mM).

Fast protein liquid chromatography (FPLC, ÄKTA) was used for protein purification. Protein fractions were detected at λ = 280 nm. Protein concentrations in the cell lysates and purified fractions were determined by using the Bradford assay and bovine serum albumin as standard (19).

Western blotting

Gel-fractionation of rPD-1 was performed by electrophoresis using 11% polyacrylamide gels containing sodium dodecyl sulfate (SDS) according to the Laemmli method using a Bio-Rad electrophoresis apparatus (Bio-Rad, USA) (20). Antigens were blotted onto nitrocellulose membranes using an immunoblotting device (Bio-Rad, USA) according to a previously published method (21).

For immunochemical detection of specific antigens, nitrocellulose membranes were first incubated in 1% BSA solution overnight at 4 °C and then washed thrice in buffer 1 containing 137 mM NaCl, 10 mM Na_2HPO_4, pH 7.4, and buffer 2 (137 mM NaCl, 10 mM Na_2HPO_4, pH 7.4, Tween-20). Blots were incubated for 1.5 h at 37 °C in a solution of mouse monoclonal antibodies against His-tag, used at 1:100 in buffer 2. Subsequently, the blot was rewashed and incubated in a working dilution of peroxidase-conjugated secondary antibody for 1 h at 37 °C. The substrate solution was prepared immediately before use; 0.01 g of 4-chloro-naphthol (Sigma, USA) was dissolved in 2 mL of methanol, and mixed with 18 mL of buffer 1; finally, 0.01 mL of 3% (v/v) hydrogen peroxide was added. This substrate solution was applied to the blots for visualization of the positive protein bands. The blot was placed in the substrate solution and incubated for 15 min at 20 °C until the stained spots appeared.

Nano LC and tandem mass spectrometry (nanoLC-MS/MS)

Workbench surfaces were routinely cleaned of dust using a clean, damp paper towel to avoid sample contamination with keratin. To ensure sample purity, we also used keratin-free Eppendorf tubes and barrier tips during sample preparation. Purified rPD-1 samples were fractionated using 11% SDS-PAGE. Gels were stained with Coomassie blue. Protein bands were excised precisely and transferred to keratin-free Eppendorf tubes. The excised bands were divided into small gel fragments, 1×1 mm dimensions. To destain the gel pieces off Coomassie blue, 100 µL of 100 mM ammonium bicarbonate in acetonitrile (1:1) was added, and gel fragments incubated at 37 °C for 30–40 min. After removing the supernatant, 5m M DTT was added to each tube and incubated at 60 °C for 10 min to reduce the disulfide bonds. DDT was removed, and 100 µL of 100 mM iodoacetamide was added and incubated at 37 °C for 15 min to alkylate the reduced cysteine residues of the proteins. Excess of reagent was removed, and the gel pieces were washed twice in 100 µL of 50 mM ammonium bicarbonate. To remove residual iodoacetamide, gel pieces were subjected to two cycles of dehydration in 200 µL of 100% acetonitrile and rehydration in 50 mM ammonium bicarbonate in water. The gel pieces were dehydrated in 100% acetonitrile for 3–5 min to reduce the size of the gel pieces; acetonitrile was removed, and tubes dried for 5 min. Finally, 2 µL of 100 ng/µL trypsin and 50 µL of 50 mM ammonium bicarbonate were added, and tubes incubated overnight at 37 °C for trypsin digestion. On the following day, the supernatant containing the peptide mixtures resulting from trypsin digestion was transferred to clean Eppendorf tubes. For a second extraction of digested peptides, the remaining gel pieces were washed in 50 µL of 50 mM ammonium bicarbonate, incubated for 15–20 min, and supernatant transferred into the same tube containing the peptide mixture from the previous extraction. The contents of the tubes were dried using a vacuum concentrator at 45 °C for 30–60 min. After complete removal of water, the resultant residue (containing peptides) was dissolved in 10 µL of a 0.1% trifluoroacetic acid, and the soluble peptide mixture was desalted using a Zip-tip kit (Millipore Ziptips Micro-C18, 0.2 µL bed, Z720003- 96EA).

The resulting mixture of trypsin-digested peptides was separated using high-performance liquid chromatography (HPLC) and analyzed

by in-line tandem mass spectrometry. For LC-MS/MS, an Acclaim™ PepMap™ 100 C18 pre-column (5 mm × 300 cm; 5 µm particles; Thermo Fisher Scientific) was used with a Dionex HPLC pump (Ultimate 3000 RSLC nano System, Thermo Fisher Scientific). The peptide mixture was separated on an Acclaim™ PepMap™ RSLC column (15 cm × 75 µm, 2 µm particle size; Thermo Fisher Scientific) using a 75-min multistage acetonitrile gradient (buffer A, 0.1% formic acid; buffer B, 90% acetonitrile/10% H_2O in 0.1% formic acid) at a flow rate of 0.3 µL/min. The gradient program for buffer B was: 0 min—2%, 10 min—2%, 58 min—50%, 59 min—99%, 69 min—99%, 70 min—2.0%, 75 min—2.0%. The unmodified Captive Spray ion source (Capillary 1300 V, dry gas 3.0 L/min, dry temperature 150 °C) was used to interface the chromatography system to the Impact II (Bruker). Subjecting the mixture of digested peptides to chromatography ensured removal of low-molecular-weight impurities. The tandem MS/MS conditions were as follows: two of the most intense precursor ions to obtain sample data were selected for subsequent fragmentation with a full-time cycle of 3 s. The mass range was from 150 to 2,200 m/z under the positive ion mode. The Mascot software was used to search the SwissProt database.

Results

Design and de novo synthesis of rPD-1

To obtain rPD-1, which could potentially infiltrate tumor tissues better than therapeutic antibodies and ultimately react with the ligand PD-L1, the amino acid sequence of the extracellular domain of PD-1 was used (Fig. 1).

The two-step polymerase chain reaction and cloning produced the expected product of 500 base pairs, which corresponds well with the predicted size of the human rPD-1 DNA sequence.

Nucleotide sequencing of the *rPD-1* gene of 500 bp size was generally satisfactory except for one error, suggesting an error rate of 0.9 per kb. This error was a deletion in the nucleotide sequence. We designed and obtained two primers and performed PCR to eliminate this deletion error successfully.

Transformation of gene construction and establishing the E. coli strain producing rPD-1

Transformation experiments allowed us to obtain the *E. coli* BL21/ pET28/ rPD-1 strain, which could produce the human rPD-1. To detect protein expression, *E. coli* were cultured in the LB medium with 0.2 mM IPTG. After addition of IPTG, *E. coli* were taken at different time points, sonicated, lysed, and subjected to SDS-PAGE. We found that rPD-1 was expressed 2 h after IPTG addition (Fig. 2A, lane 2), and the molecular mass of the protein was ~21 kDa, consistent with the theoretical mass of rPD-1. rPD-1 was overexpressed 4 h after IPTG addition but remained unchanged at 25 °C up to 12 h after IPTG addition (Fig. 2A, lanes 3–5). rPD-1 was mainly expressed in inclusion bodies because it was detected only in the precipitate (data not shown). Additionally, we used the anti-His-tag monoclonal antibody in western blotting of rPD-1 samples (Fig. 2B) to confirm its expression. Western blotting confirmed the presence of the hexa histidine tag in a protein with a molecular mass of ~21 kDa, which corresponds to the predicted molecular mass of rPD-1.

Isolation and purification of rPD-1

To optimize isolation and purification of rPD-1, the BL21/ pET28/ rPD-1 *E. coli* were cultured in LB medium containing kanamycin and various IPTG concentration sat 0.1 mM, 0.25 mM, 0.5 mM, 1 mM and at two different temperatures, 25 and 37 °C. Finally, the relative amount of rPD-1 was measured in the *E. coli* lysates. We found that the conditions for optimal expression of rPD-1 were the media containing 0.2 mM IPTG and incubation at 25 °C (Table 2).

Table 2. Relative amounts of recombinant proteins (%) in insoluble fractions of lysates of producer strains under various conditions of expression induction

Concentration of IPTG		0.1 mM	0.2 mM	0.5 mM	1 mM
pET28/rPD-1 yield	25 ºC	50%	50%	30%	10%
*n/d—not detected	37 ºC	8%	8%	n/d*	n/d*

```
                          1                                                  50
PD-1 homo sp.      (1)    MQIPQAPWPVVWAVLQLGWRPGWFLDSPDRPWNPPTFSPALLVVTEGDNA
Rec Human PD-1     (1)    ----------------------LDSPDRPWNPPTFSPALLVVTEGDNA
    Consensus      (1)                           LDSPDRPWNPPTFSPALLVVTEGDNA
                          51                                                 100
PD-1 homo sp.      (51)   TFTCSFSNTSESFVLNWYRMSPSNQTDKLAAFPEDRSQPGQDCRFRVTQL
Rec Human PD-1     (27)   TFTCSFSNTSESFVLNWYRMSPSNQTDKLAAFPEDRSQPGQDCRFRVTQL
    Consensus      (51)   TFTCSFSNTSESFVLNWYRMSPSNQTDKLAAFPEDRSQPGQDCRFRVTQL
                          101                                                150
PD-1 homo sp.      (101)  PNGRDFHMSVVRARRNDSGTYLCGAISLAPKAQIKESLRAELRVTERRAE
Rec Human PD-1     (77)   PNGRDFHMSVVRARRNDSGTYLCGAISLAPKAQIKESLRAELRVTERRAE
         nsus      (101)  PNGRDFHMSVVRARRNDSGTYLCGAISLAPKAQIKESLRAELRVTERRAE
                          151                                                200
PD-1 homo sp.      (151)  VPTAHPSPSPRPAGQFQTLVVGVVGGLLGSLVLLVWVLAVICSRAARGTI
Rec Human PD-1     (127)  VPTAHPSPSPRPAGQFQHHHHHH--------------------------
    Consensus      (151)  VPTAHPSPSPRPAGQFQ
                          201                                                250
PD-1 homo sp.      (201)  GARRTGQPLKEDPSAVPVFSVDYGELDFQWREKTPEPPVPCVPEQTEYAT
Rec Human PD-1     (150)  --------------------------------------------------
    Consensus      (201)
                          251                                288
PD-1 homo sp.      (251)  IVFPSGMGTSSPARRGSADGPRSAQPLRPEDGHCSWPL
Rec Human PD-1     (150)  -----------------------------------
      nsensus      (251)
```

Fig. 1. Amino acid sequence of the extracellular domain of the human PD-1 receptor (yellow color).

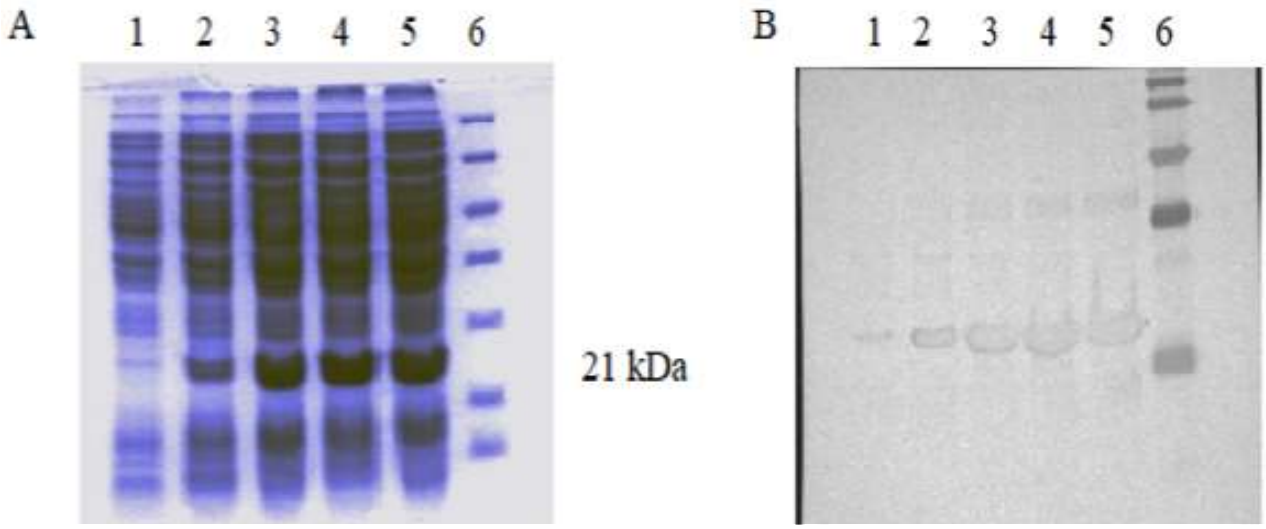

Fig. 2. SDS-PAGE (A) and western blotting (B) of total proteins expressed and extracted from the BL21/ pET28/ rPD-1 *E. coli*. Lane 1—*E. coli* culture without IPTG; Lane 2—protein expression 2 h after IPTG addition; Lane 3—protein expression 4 h after IPTG addition; Lane 4- protein expression after 6 h incubation with IPTG; Lane 5—protein expression after 12-h incubation with IPTG; Lane 6—molecular-weight markers.

After purification of rPD-1 by nickel–Sepharose chromatography and elution using 200 mM imidazole in buffer, we used SDS-PAGE and Coomassie staining to visualize the rPD-1 bands. The homogeneity of purified rPD-1 was confirmed, and an example is presented in Fig. 3.

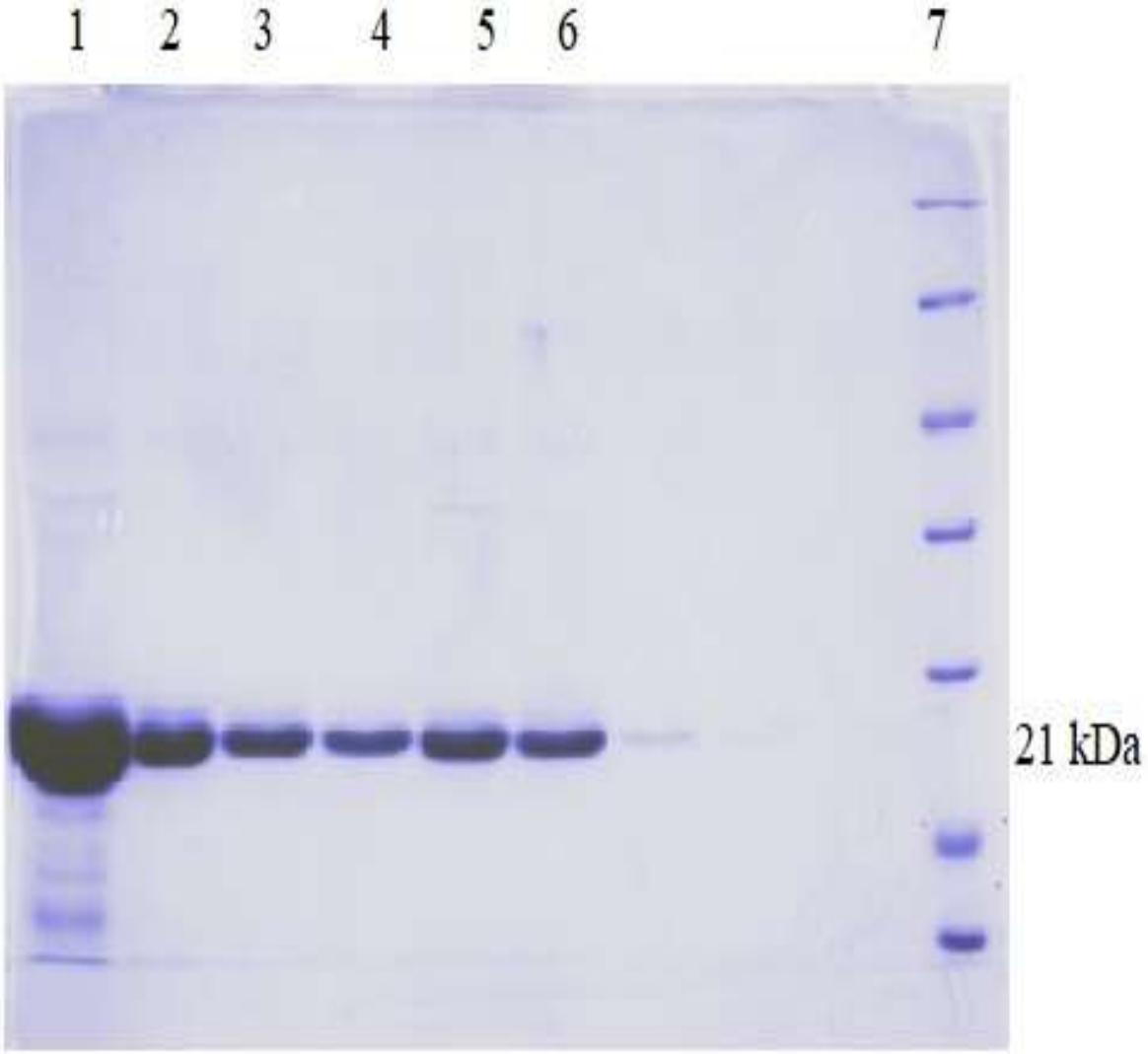

Fig. 3. SDS-PAGE-purified rPD-1 expressed by the BL21/ pET28/ rPD-1 *E. coli*. Lanes 1–6, purified fractions of rPD-1; Line 7, molecular-weight markers.

LC-MS/MS analysis of rPD-1

LC-MS/MS was used to confirm the identity of rPD-1. MS/MS spectra of peaks corresponding to fragmented ions of peptides derived from trypsin-digested rPD-1 were identified following SDS-PAGE, trypsin digestion, and chromatographic separation. Trypsin-digested peptides are characterized by lysine or arginine residues at the C-terminus. The MS/MS spectra were converted to mgf files using the Data Analysis program. These files were submitted to the Mascot search engine, which compares the experimental data with theoretical mass spectra using available sequence databases of amino acids, such as NCBI or SwissProt.

As a result, the Mascot output included 38 of the most probable proteins, corresponding to cumulative MS/MS spectra. The highest score (4,950) corresponded to only one protein, rPD-1. Representative MS/MS spectra of MSPSNQTDKLAAFPEDR, LAAFPEDR, and NDSGTYLCGAISLAPK peptides of rPD-1 and their fragmentation ions are presented in Fig. 4.

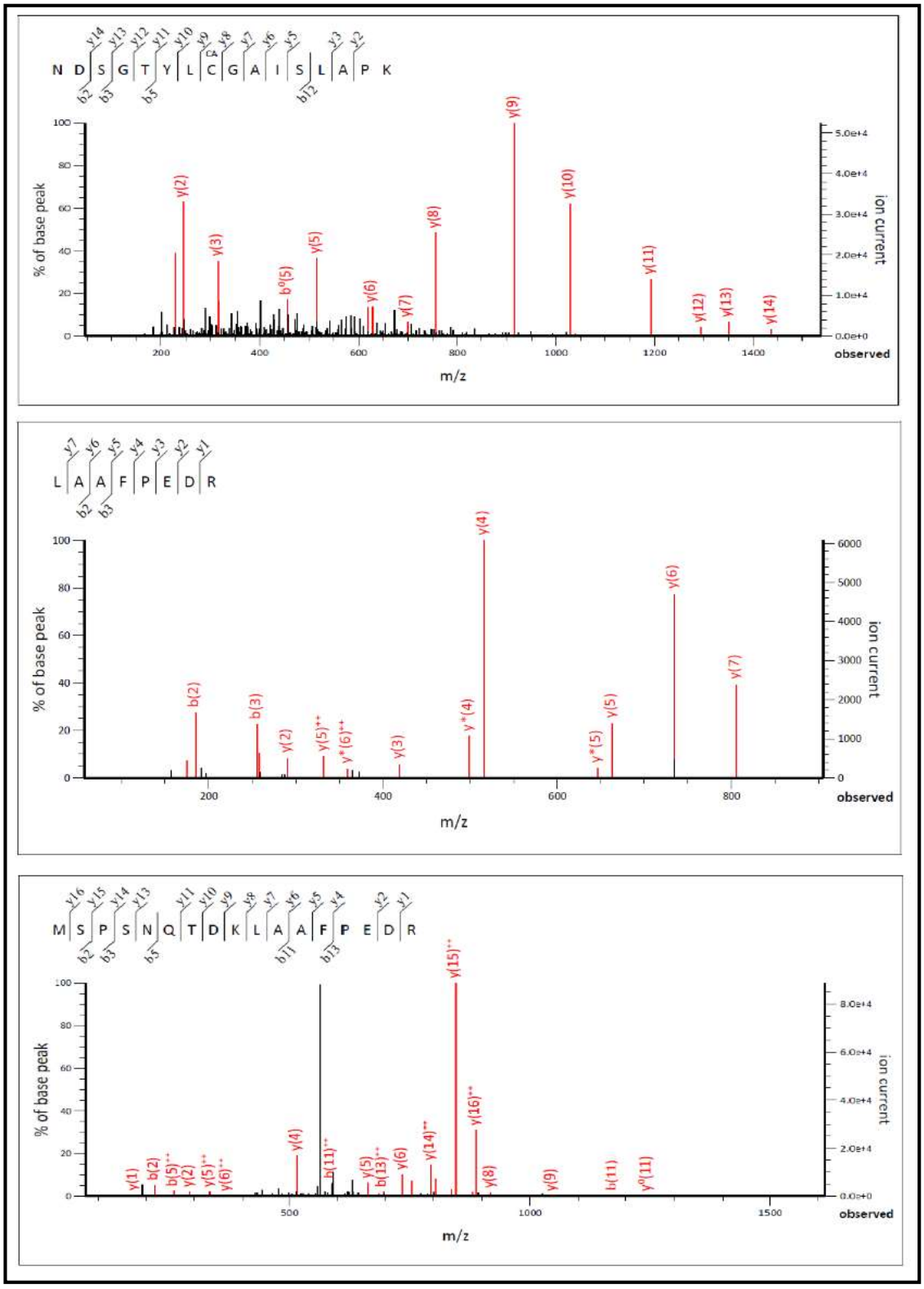

Fig. 4. MS/MS spectra of fragmented peptides derived from trypsin-digested rPD-1.

Discussion

PD-1–PD-L1 and PD-1–PD-L2 interactions play critical roles in immunity against infection but negative roles in carcinogenesis. Structural studies of PD-1–PD-L1 interaction have confirmed a 1:1 stoichiometry with a significant interaction interface. Large hydrophobic surfaces corresponding to Ig-like, V-type domains dominate the PD-1–PD-L1 interface. When forming the complex, the long axes of PD-1 and PD-L1 position almost perpendicularly to each other, facilitating interaction across almost the entire surface of the "frontal" PD-1–PD-L1 interface (22).

A mutant version of PD-1 termed high-affinity consensus (HAC) PD-1, synthesized by directed molecular evolution and phage display, was shown to block the PD-1–PD-L1 or PD-1–PD-L2 interactions because it has higher affinity to ligands than wild-type PD-1. Thus, the mutant HAC PD-1 can possibly be modified to be applied as a potential therapeutic agent in the clinics. Similarly, additional strategies for developing immune-checkpoint inhibitors, such as for CTLA-4 and Tim-3 or their ligands, have been proposed (23).

A structural study showed that interactions between human HAC PD-1 and PD-L1 are mostly similar to interactions between human wild-type PD-1 and human wild-type PD-L1 but differ in some critical areas. HAC PD-1 engages through a much more extensive network of polar contacts with PD-L1 than does the wild-type PD-1. The wild-type PD-1 was reportedly less ordered, with loops adopting a wide range of conformations in addition to those seen previously in static crystal structures. In contrast, the PD-1 mutant is more modestly flexible than the wild-type PD-1, especially in the b4–b5 loop. The authors concluded that their observations arise from a single non-conservative substitution, Met70Glu, which holds the b4– b5 loop in an open, binding-competent conformation by a stable salt-bridge interaction with Arg139 (24).

Considering the above background, here, we prepared the recombinant extracellular domain of the PD-1 receptor aiming for its more extensive use as a future therapeutic drug. We synthesized rPD-1 by using the Phusion® polymerase and cloned rPD-1 into expression vectors transformed into *E. coli* strain BL21 (DE3). We assessed and confirmed the rPD-1 expression and optimized the conditions for isolation and purification of rPD-1.

Notably, various approaches have been developed for synthesizing DNA using more accurate Pfu and Phusion® polymerases. According to Dolgova and Stukolova, average error rates during amplification of a 581-bp DNA fragment were 2.2 ± 0.837 and 0.6 ± 0.548 for Pfu and Phusion®, respectively, indicating that Phusion® is three times more efficient than Pfu. This significant difference can be explained by the fact that only Phusion® has a DNA-binding domain fused to the *Pyrococcus*-like proof-reading polymerase. Using Phusion® reduces the number of clones needed to find the correct sequence of a target gene and eliminates the nucleotide-editing stage (25).

We found that the BL21/ pET28/ rPD-1 *E. coli* could produce rPD-1 in high yields despite the fact that rPD-1 was formed within inclusion bodies as an insoluble protein. We solubilized rPD-1 in 8 M urea and subjected it to refolding by ion-exchange chromatography on a nickel–Sepharose column. This method allowed using an initial high concentration of the protein, which was effectively refolded while simultaneously being separated from high-molecular-weight protein aggregates. Refolding was achieved by spatially separating the rPD-1 molecules from each other through the pores of the column and a gradual decrease in concentration of the denaturing agent. Denatured rPD-1 has been shown to re-form its unique native spatial conformation by refolding on a column. Because renatured rPD-1 had a high binding affinity with PD-L1, we hypothesize that rPD-1 glycosylation was unnecessary for ligand binding. Our results indicate that the prokaryotic expression system can be used to obtain biologically active soluble rPD-1 using appropriate refolding strategies (26).

In summary, we successfully prepared the recombinant extracellular domain of the PD-1, which we believe will be useful for the generation of either diagnostic or therapeutic monoclonal antibodies and can also be used as a protein therapeutic.

Acknowledgment

This research was performed within the framework of the budget program 217 of the Ministry of Education and Science, the Republic of Kazakhstan on the hybrid cells producing monoclonal antibodies against the receptor for programmed cell death of PD-1 factor project No. AP05130036, "Obtaining a strain of reducing immunity against cancer" for the period 2018–2020.

On behalf of all authors, the corresponding author states that there is no conflict of interest.

References

1. Mamalis A, Garcha M, Jagdeo J .Targeting the PD-1 pathway: a promising future for the treatment of melanoma. Arch. Dermatol. Res.2 014;306:511-19.
2. Barber DL, Wherry EJ, Masopust D, Zhu B, Allison JP, Sharpe AH, Freeman GJ, Ahmed R.Restoring function in exhausted CD8 T cells during chronic viral infection. Nature. 2006;439:682-87.
3. Francisco LM, Sage PT, Sharpe AH. The PD-1 pathway in tolerance and autoimmunity. Immunol.Rev.2010;236:219-42,
4. Dong Y, Sun Q, Zhang X. PD-1 and its ligands are important immune checkpoints in cancer. Oncotarget.2017;8:2171-86.
5. Lorenz U. SHP-1 and SHP-2 in T cells: two phosphatases functioning at many levels. Immunol. Rev. 2009;228:342-59.
6. Shinohara T, Taniwaki M, Ishida Y, Kawaichi M, Honjo T. Structure and chromosomal localization of the human PD-1 gene (PDCD1). Genomics. 1994;23:704-706.
7. Starr R, Willson TA, Viney EM, Murray LJ, Rayner JR, Jenkins BJ, Gonda TJ, Alexander WS, Metcalf D, Nicola NA, Hilton DJ. A family of cytokine-inducible inhibitors of signaling. Nature. 1997;387:917-21.
8. Agata Y, Kawasaki A, Nishimura H, Ishida Y, Tsubata T, Yagita H, Honjo T.Expression of the PD-1 antigen on the surface of stimulated mouse T and B lymphocytes. Int.Immunol. 1996;8:765-72.
9. Matsuzaki J, Gnjatic S, Mhawech-Fauceglia P, Beck A, Miller A, Tsuji T, Eppolito C, Qian F, LeleS, Shrikant P, Old LJ, Odunsi K. Tumor-infiltrating NY-ESO-1–specific CD8 + T cells are negatively regulated by LAG-3 and PD-1 in human ovarian cancer. Proc. Natl. Acad. Sci. USA. 2010;107:7875-80.
10. Kao C, Oestreich KJ, Paley MA, Crawford A, Angelosanto JM, Ali MA, Intlekofer AM, Boss JM, Reiner SL, Weinmann AS, Wherry EJ. Transcription factor T-bet represses expression of the inhibitory receptor PD-1 and sustains virus-specific CD8+ T cell responses during chronic infection. Nat. Immunol. 2011;12:663-71.
11. Sanmamed MF, Chen L. Inducible expression of B7-H1 (PD-L1) and its selective role in tumor site immune modulation. Cancer J. 2014;20:256-61.
12. Larkin J, Chiarion-Sileni V, Gonzalez R, Grob JJ, Cowey CL, Lao CD, Schadendorf D, Dummer R,Smylie M, Rutkowski P, Ferrucci PF, Hill A, et al.Combined nivolumab and ipilimumab or monotherapy in untreated melanoma. N. Engl. J. Med.2015;373:23-4.
13. Motzer RJ, Escudier B, McDermott DF, George S, Hammers HJ, Srinivas S, Tykodi SS, Sosman JA, Procopio G, Plimack ER, Castellano D, Choueiri TK, et al. Nivolumab versus Everolimus in advanced renal-cell carcinoma. N. Engl. J. Med.2015;373:1803-13.
14. Reck M, Rodríguez-Abreu D, Robinson AG, Hui R, Csőszi T, Fülöp A, Gottfried M, Peled N, Tafreshi A, Cuffe S, O'Brien M, Rao S, Hotta K, Leiby MA, Lubiniecki GM, Shentu Y, Rangwala R, Brahmer JR. Pembrolizumab versus chemotherapy for PD-L1–positive non–small-cell lung cancer. N. Engl. J. Med.2016;375:1823-33.
15. Sharma P, Callahan MK, Bono P, Kim J, Spiliopoulou P, Calvo E, Pillai RN, Ott PA, de Braud F, Morse M, Le DT, Jaeger D, Chan E, Harbison C, Lin CS, Tschaika M, Azrilevich A, Rosenberg JE. Nivolumab monotherapy in recurrent metastatic urothelial carcinoma (CheckMate 032): a multicentre, open-label, two-stage, multi-arm, phase 1/2 trial. Lancet Oncol.2016;17:1590-98.
16. Morales-Betanzos CA, Lee H, Gonzalez Ericsson PI, Balko JM, Johnson DB, Zimmerman LJ, Liebler DC. Quantitative mass spectrometry analysis of PD-L1 protein expression, N-glycosylation and expression stoichiometry with PD-1 and PD-L2 in human melanoma. Mol. Cell Proteomics.2017;16:1705-17.
17. Shimizu T, Seto T, Hirai F, Takenoyama M, Nosaki K, Tsurutani J, Kaneda H, Iwasa T, Kawakami H, Noguchi K, Shimamoto T, Nakagawa K. Phase 1 study of pembrolizumab (MK-3475; anti-PD-1 monoclonal

antibody) in Japanese patients with advanced solid tumors. Invest. New Drugs. 2016;34:347-54.
18. Maute RL, Gordon SR, Mayer AT, McCracken MN, Natarajan A, Ring NG, Kimura R, Tsai JM, Manglik A, Kruse AC, Gambhir SS, Weissman IL, Ring AM. Engineering high-affinity PD-1 variants for optimized immunotherapy and immuno-PET imaging. Proc. Natl. Acad. Sci. USA. 2015;112:6506–14.
19. Bradford MM. A rapid and sensitive method for the quantitation of microgram quantities of protein utilizing the principle of protein-dye binding. Anal. Biochem.1976;72:248–54.
20. Laemmli UK. Cleavage of structural proteins during the assembly of the head of bacteriophage T4. Nature.1970;227:680–85.
21. Towbin H, Staehelin T, Gordon J. Electrophoretic transfer of proteins from polyacrylamide gels to nitrocellulose sheets: procedure and some applications. Proc. Natl. Acad. Sci. USA. 1979;76:4350–54.
22. Zak KM, Grudnik P, Magiera K, Dömling A, Dubin G, Holak TA. Structural biology of the immune checkpoint receptor PD-1 and its ligands PD-L1/PD-L2. Structure. 2017;25:116374.
23. Li Y, Liang Z, Tian Y, Cai W, Weng Z, Chen L, Zhang H, Bao Y, Zheng H, Zeng S, Bei C, Li Y. High-affinity PD-1 molecules deliver improved interaction with PD-L1 and PD-L2. Cancer Sci.2018;109:2435–45.
24. Pascolutti R, Sun X, Kao J, Maute RL, Ring AM, Bowman GR, Kruse AC. Structure and dynamics of PD-L1 and an ultra-high-affinity PD-1 receptor mutant. Structure.2016;24:1719–28.
25. Dolgova AS, Stukolova OA. High-fidelity PCR enzyme with DNA-binding domain facilitates de novo gene synthesis. 3 Biotech. 2017;7:128.
26. Xu L, Liu Y, He X. Expression and purification of soluble human programmed death-1 in Escherichia coli. Cell Mol. Immunol. 2006;3:139–4**.**